Spin-Orbit Coupling in Ferromagnetic Nickel

J. Bünemann,[1] F. Gebhard,[1] T. Ohm,[2] S. Weiser,[2] and W. Weber[2]

[1]*Fachbereich Physik and Material Sciences Center, Philipps–Universität Marburg, D-35032 Marburg, Germany*

[2]*Fachbereich Physik, Universität Dortmund, D-44221 Dortmund, Germany*

(Received 14 April 2008; published 4 December 2008)

We use the Gutzwiller variational theory to investigate the electronic and magnetic properties of fcc nickel. Our particular focus is on the effects of the spin-orbit coupling. Unlike standard relativistic band-structure theories, we reproduce the experimental magnetic-moment direction and we explain the change of the Fermi-surface topology that occurs when the magnetic-moment direction is rotated by an external magnetic field. The Fermi surface in our calculation deviates from early de Haas–van Alphen results. We attribute these discrepancies to an incorrect interpretation of the raw de Haas–van Alphen data.

DOI: 10.1103/PhysRevLett.101.236404 PACS numbers: 71.20.Be, 71.10.Fd, 71.27.+a, 75.50.Cc

The limitations of density functional theory (DFT) when treating the electronic and magnetic properties of transition metals become evident most clearly in the case of nickel. The DFT cannot reproduce gross features such as the width of the $3d$ bands (4.5 eV versus 3.3 eV experimentally [1–3]), nor important details such as the exchange splitting. The exchange splitting in the DFT is almost 0.7 eV and rather isotropic over the Fermi surface, whereas, experimentally, it is found to be much smaller and strongly orbital dependent: $\Delta_{e_g} \approx 0.17$ eV and $\Delta_{t_{2g}} \approx 0.33$ eV. As a result, even the Fermi-surface topologies do not match, because of the position of the $X_{2\downarrow}$ energy: above the Fermi energy (E_F) in DFT, yet below E_F experimentally; thus only one hole ellipsoid exists around the X point, versus two in DFT [4,5].

More limitations of DFT become evident when the effects of the spin-orbit coupling are considered. The magnetic anisotropy energy (MAE) has the wrong sign for nickel (and for cobalt), while it has the correct sign for iron, yet is too small by a factor of 3 [6]. In nickel, the easy axis is along [111] and approximately 3 μeV per atom are needed to rotate the magnetic-moment axis into the [001] direction [7,8]. Moreover, a low-temperature study of the magnetic anisotropy constants K_1, K_2, K_3 by Gersdorf [8] reveals a change in the Fermi-surface topology when the magnetic-moment axis is rotated into the [001] direction: A small second hole ellipsoid appears around the $X(001)$ point, but not around the $X(100)$ and $X(010)$ points, now inequivalent to $X(001)$ because of the underlying tetragonal symmetry.

It is generally accepted that the discrepancies between the DFT and the experimental results are mainly caused by an insufficient treatment of the electronic correlation in an effective one-particle theory. In the past, all attempts to combine the DFT with more sophisticated correlated electron theories have only led to partial improvements of the results for nickel; see, e.g., the *GW* and dynamical mean-field theory (DMFT) approximations in Refs. [9–11]. Despite their merits, the DMFT calculations have, for numerical reasons, an energetic resolution which is too low to tackle the subtle electronic properties of nickel. A high resolution is mandatory, in particular, for a proper treatment of the spin-orbit coupling effects in transition metals.

In a recent work [4] we showed that a generalized Gutzwiller theory provides a consistent picture of the quasiparticle band structure of nickel. Neglecting spin-orbit coupling, all basic problems of the DFT calculations on nickel have been resolved. Our theory employed approximately 2^{10} variational parameters representing the occupancies of all atomic multielectron states within an open $3d$ shell (see below).

In this Letter we present results for the case when spin-orbit coupling is included. In order to cope with this complication, the Gutzwiller theory had to be extended [12] to allow for rotations in the eigenvector space of the atomic multielectron states, resulting in many more variational parameters. Employing this generalization we obtain the correct MAE, and, more importantly, reproduce the change in the Fermi-surface topology found by Gersdorf.

To investigate transition metals we start from multiband Hubbard models of the general form

$$\hat{H} = \sum_{i \neq j;\sigma,\sigma'} t_{i,j}^{\sigma,\sigma'} \hat{c}_{i,\sigma}^{\dagger} \hat{c}_{j,\sigma'} + \sum_i \hat{H}_{\mathrm{loc},i} = \hat{H}_0 + \hat{H}_{\mathrm{loc}}. \quad (1)$$

Here, the first term describes the hopping of electrons between spin-orbital states σ, σ' on lattice sites i, j, respectively. The Hamiltonian $\hat{H}_{\mathrm{loc},i} = \hat{H}_{C,i} + \hat{H}_{\mathrm{cf},i} + \hat{H}_{\mathrm{SO},i}$ contains all local terms; i.e., the two-particle Coulomb interaction $\hat{H}_{C,i}$, the crystal-field energies $\hat{H}_{\mathrm{cf},i}$, and the spin-orbit coupling $\hat{H}_{\mathrm{SO},i}$. In the case of nickel, we work with a basis of $3d$, $4s$, and $4p$ orbitals.

The hopping parameters in the one-particle Hamiltonian $\hat{H}_0$ and the crystal-field energies in $\hat{H}_{\mathrm{cf}}$ are determined by means of a tight-binding fit to the paramagnetic DFT band structure [4,12]. In principle, a self-consistent "local density approximation (LDA) + Gutzwiller" scheme as proposed in Ref. [13] could be employed. For nickel, we do not expect significant changes of the results because the

band renormalization and the exchange splittings are moderate. Moreover, in the presence of the spin-orbit coupling the LDA + Gutzwiller method is numerically very demanding.

Because of the large bandwidth of the $4s$ and $4p$ bands, only the Coulomb interaction within the $3d$ shell is taken into account. The spherical approximation is used; i.e., we express the Coulomb interaction through the three Racah parameters A, B, and C [14]. In order to reproduce the experimental d bandwidth in our approach, we need a Racah parameter $A = 9$ eV. Note that the results do not depend on the value of A very sensitively; i.e., we find similar results for a range of $A \approx 8$–10 eV. The value of A would be much smaller if we used a more restricted basis set; e.g., $A \approx 3$–4 eV reproduces the correct bandwidth renormalization for an (artificial) pure $3d$-band model. The Racah parameters B and C are assumed to be close to their atomic values [14], $B = 85$ meV and $C = 400$ meV. The spin-orbit coupling parameter ζ in the spin-orbit Hamiltonian

$$\hat{H}_{\mathrm{SO},i} = \sum_{\sigma\sigma'} \frac{\zeta}{2} \langle \sigma | \hat{l}_x \tilde{\sigma}_x + \hat{l}_y \tilde{\sigma}_y + \hat{l}_z \tilde{\sigma}_z | \sigma' \rangle \hat{c}^{+}_{i,\sigma} \hat{c}_{i,\sigma'} \quad (2)$$

is chosen as $\zeta = 80$ meV. Note that the Hamiltonian (2) only contains d orbitals.

In the Gutzwiller theory, the variational ansatz [12,15,16]

$$|\Psi_G\rangle = \hat{P}_G |\Psi_0\rangle = \prod_i \hat{P}_i |\Psi_0\rangle \quad (3)$$

is used to investigate the multiband Hubbard model (1). Here, $|\Psi_0\rangle$ is a normalized single-particle product state and the local Gutzwiller correlator is defined as

$$\hat{P}_i = \sum_{\Gamma,\Gamma'} \lambda_{\Gamma,\Gamma'} |\Gamma\rangle_{ii} \langle \Gamma'|. \quad (4)$$

The states $|\Gamma\rangle_i$ form some arbitrary basis of the atomic Hilbert space on site i and the (complex) numbers $\lambda_{\Gamma,\Gamma'}$ are variational parameters. For nickel, we work with a correlation operator (4) in which the states $|\Gamma\rangle_i$ are the eigenstates of the atomic Hamiltonian $\hat{H}_{C,i}$. The nondiagonal elements of the variational parameter matrix $\lambda_{\Gamma,\Gamma'}$ are assumed to be finite only for states $|\Gamma\rangle$, $|\Gamma'\rangle$ which belong to the same atomic multiplet. This is consistent with the spherical approximation for the Coulomb interaction. In the case of nickel, it is sufficient to work with nondiagonal parameters $\lambda_{\Gamma,\Gamma'}$ in the d^7, d^8, and d^9 shells. We assume translational invariance and skip lattice indices for local quantities.

The expectation value of the Hamiltonian (1) can be calculated analytically for the Gutzwiller wave function (3) in the limit of infinite spatial dimensions [16]. We use the exact results in this limit as an approximation for our three-dimensional model system. In infinite dimensions one finds

$$\langle \hat{H}_{\mathrm{loc},i} \rangle_{\Psi_G} = \sum_{\Gamma_1 \ldots \Gamma_4} \lambda^{*}_{\Gamma_2,\Gamma_1} \lambda_{\Gamma_3,\Gamma_4} E^{\mathrm{loc}}_{\Gamma_2,\Gamma_3} m^{0}_{\Gamma_1,\Gamma_4} \quad (5)$$

for the expectation value of $\hat{H}_{\mathrm{loc},i}$ in (1), where $E^{\mathrm{loc}}_{\Gamma_2,\Gamma_3} \equiv \langle \Gamma_2 | \hat{H}_{\mathrm{loc},i} | \Gamma_3 \rangle$ and $m^{0}_{\Gamma_1,\Gamma_4} \equiv \langle (|\Gamma_1\rangle\langle\Gamma_4|) \rangle_{\Psi_0}$. These local expectation values are readily calculated by means of Wick's theorem. For the expectation value of a hopping operator in (1) one finds

$$\langle \hat{c}^{\dagger}_{i,\sigma_1} \hat{c}_{j,\sigma_2} \rangle_{\Psi_G} = \sum_{\sigma'_1,\sigma'_2} q^{\sigma'_1}_{\sigma_1} (q^{\sigma'_2}_{\sigma_2})^{*} \langle \hat{c}^{\dagger}_{i,\sigma'_1} \hat{c}_{j,\sigma'_2} \rangle_{\Psi_0}. \quad (6)$$

The renormalization matrix $q^{\sigma'}_{\sigma}$ in (6) can be calculated most easily when an orbital basis is used which has a diagonal local density matrix with respect to $|\Psi_0\rangle$, $C^{0}_{\sigma,\sigma'} \equiv \langle \hat{c}^{\dagger}_{i,\sigma} \hat{c}_{i,\sigma'} \rangle_{\Psi_0} = \delta_{\sigma,\sigma'} n^{0}_{\sigma}$. If $C^{0}_{\sigma,\sigma'}$ is nondiagonal for a one-particle product state $|\Psi_0\rangle$ one can always transform the orbital basis in order to make $C^{0}_{\sigma,\sigma'}$ diagonal. Then, the renormalization matrix in (6) reads

$$q^{\sigma'}_{\sigma} = \frac{1}{n^{0}_{\sigma'}} \sum_{\Gamma_1 \ldots \Gamma_4} \lambda^{*}_{\Gamma_2,\Gamma_1} \lambda_{\Gamma_3,\Gamma_4} \langle \Gamma_2 | \hat{c}^{\dagger}_{\sigma} | \Gamma_3 \rangle \langle (|\Gamma_1\rangle\langle\Gamma_4| \hat{c}_{\sigma'}) \rangle_{\Psi_0}, \quad (7)$$

where, again, the expectation value with respect to $|\Psi_0\rangle$ is calculated with Wick's theorem.

The variational ground-state energy must be minimized with respect to the variational parameters $\lambda_{\Gamma,\Gamma'}$ and the one-particle product wave functions $|\Psi_0\rangle$. The optimum state $|\Psi_0\rangle$ is the ground state of the effective one-particle Hamiltonian [12,17]

$$\hat{H}^{\mathrm{eff}}_{0} = \sum_{i \neq j;\sigma,\sigma'} \tilde{t}^{\sigma,\sigma'}_{i,j} \hat{c}^{\dagger}_{i,\sigma} \hat{c}_{j,\sigma'} + \sum_{i;\sigma,\sigma'} \eta_{\sigma,\sigma'} \hat{c}^{\dagger}_{i,\sigma} \hat{c}_{i,\sigma'} \quad (8)$$

with the renormalized hopping matrix elements

$$\tilde{t}^{\sigma_1,\sigma_2}_{i,j} = \sum_{\sigma'_1,\sigma'_2} q^{\sigma_1}_{\sigma'_1} (q^{\sigma_2}_{\sigma'_2})^{*} t^{\sigma'_1,\sigma'_2}_{i,j} \quad (9)$$

and the Lagrange parameters $\eta_{\sigma,\sigma'}$ which are used to optimize the energy with respect to the local density matrix $C^{0}_{\sigma,\sigma'}$. Within a Landau Fermi-liquid approach one can further show [12,17] that the eigenvalues $E_{\gamma}(k)$ of $\hat{H}^{\mathrm{eff}}_{0}$ are the quasiparticle excitation energies that can be compared, for example, to angle-resolved photoemission spectroscopy experiments. Most important for the quasiparticle band structure are the Lagrange parameters $\eta^{d}_{\sigma,\sigma'}$ for the d orbitals. The two (diagonal) Lagrange parameters for the s and p orbitals are adjusted in order to fix the total d-electron number [18].

The inclusion of spin-orbit coupling complicates the numerical minimization significantly. Both the d part of the local density matrix $C^{0}_{\sigma,\sigma'}$ and of the hopping renormalization matrix (7) are no longer diagonal. The number n_{ie} of independent elements depends on the magnetic-moment direction; we find $n_{\mathrm{ie}} = 22$ for $\vec{\mu} \parallel [111]$ and $n_{\mathrm{ie}} = 18$ for $\vec{\mu} \parallel [001]$. As a consequence of the reduced

symmetry, we could work with up to n_{ie} independent d-shell Lagrange parameters $\eta^{d}_{\sigma,\sigma'}$ in order to minimize the total energy. Numerically, however, such a minimization would be quite costly since each variation of these parameters involves many momentum-space integrations. We therefore work with a simplified effective Hamiltonian $\hat{\tilde{H}}^{\mathrm{eff}}_{0}$ that contains effective parameters only for all physically relevant one-particle terms.

In cubic symmetry, there exist only four independent matrix elements of the local (d electron) density matrix. The trace of the matrix is fixed by the total d-electron number. The three remaining matrix elements are governed by parameters $\eta^{d}_{\sigma,\sigma'}$ which are given by the orbital-dependent exchange fields $\Delta_{t_{2g}}, \Delta_{e_g}$ and the effective crystal-field splitting $\epsilon^{\mathrm{eff}}_{\mathrm{CF}}$. The noncubic symmetry resulting from the addition of the spin-orbit coupling adds many more formally independent $\eta^{d}_{\sigma,\sigma'}$ terms. Both for $\vec{\mu} \parallel [001]$ (tetragonal symmetry) and for $\vec{\mu} \parallel [111]$ (trigonal symmetry) there are two more exchange fields and two more crystal-field splittings. All these eight terms are included in our simplified effective Hamiltonian $\hat{\tilde{H}}^{\mathrm{eff}}_{0}$. In the spirit of the spherical approximation [19], a Hamiltonian $\hat{H}^{\mathrm{eff}}_{\mathrm{SO}}$ is included in $\hat{\tilde{H}}^{\mathrm{eff}}_{0}$ that has the same form as $\hat{H}_{\mathrm{SO}}$ only with ζ replaced by ζ^{eff}. As a result, we have to minimize the total energy with respect to nine ''external'' parameters in our simplified Hamiltonian $\hat{\tilde{H}}^{\mathrm{eff}}_{0}$.

The numerical minimization is much more time-consuming for a system with spin-orbit coupling than without. First, spin-orbit coupling requires the momentum-space integration to be extended from 1/48th to the full Brillouin zone. Furthermore, the small values of the MAE necessitate a much finer mesh for the momentum-space integration. Second, the energy needs to be minimized with respect to nine external variational parameters in $\hat{\tilde{H}}^{\mathrm{eff}}_{0}$. Altogether, the minimization of the total energy is approximately 10^4 times more time-consuming for a system with spin-orbit coupling than in the absence of $\hat{H}_{\mathrm{SO}}$.

We carried out the minimization of the variational energy with respect to the ''internal'' parameters $\lambda_{\Gamma,\Gamma'}$ and the external parameters for both magnetic-moment directions $\vec{\mu} \parallel [111]$ and $\vec{\mu} \parallel [001]$. The optimum value of the effective spin-orbit coupling is $\zeta_{\mathrm{eff}} \approx 68$ meV in both cases, about 15% smaller than the bare value $\zeta = 80$ meV. In our calculations for nickel, the MAE is $E_{\mathrm{MAE}} \approx 3.5\ \mu$eV per atom, quite close to the experimental value $E_{\mathrm{expt}} \approx 3.0\ \mu$eV. Note that the MAE has to be calculated quite carefully within the Gutzwiller approach. In particular, one has to keep in mind that any approximation on the parameters $\lambda_{\Gamma,\Gamma'}$ that reduces the variational flexibility may lead to a grossly overestimated MAE. This is a serious problem, in particular, in the case of iron. For nickel, however, a mixing of states $|\Gamma\rangle, |\Gamma'\rangle$ has little effect on the variational energy, and even a diagonal variational parameter matrix $\lambda_{\Gamma,\Gamma'} \sim \delta_{\Gamma,\Gamma'}$ would lead to reasonable results, i.e., $E_{\mathrm{MAE}} \approx 10\ \mu$eV per atom. The absolute value of the MAE mildly depends on the parameters for the spin-orbit coupling ζ and the Racah-C; e.g., an increase of ζ by 50% doubles the MAE. However, the sign of the MAE is a robust result of our calculation.

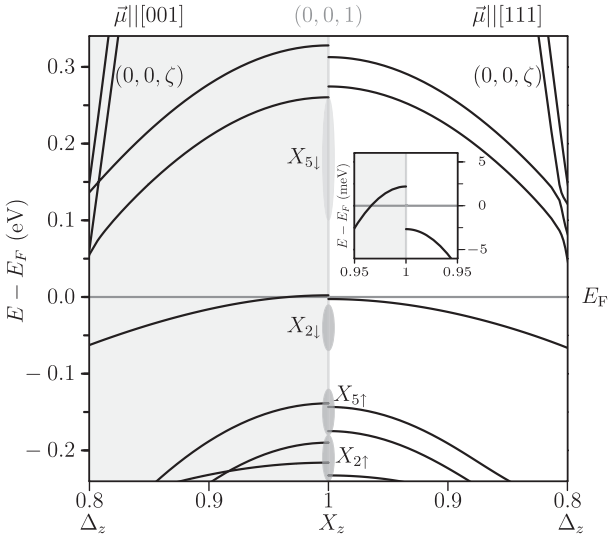

FIG. 1. Quasiparticle band structure along the Δ line around the X_z point of the Brillouin zone for magnetic-moment directions $\vec{\mu} \parallel [001]$ and $\vec{\mu} \parallel [001]$. The inset shows an enlarged view of the band structure around the Fermi energy which displays the additional hole ellipsoid for $\vec{\mu} \parallel [001]$ more clearly.

In Figs. 1 and 2 we show the quasiparticle band structure that arises from our calculation around the X points $X_z \equiv (001)$ and $X_x \equiv (100)$. When the magnetic moment is along the easy axis, the band structure around both X points coincides and the minority state $X_{2\downarrow}$ is below the Fermi

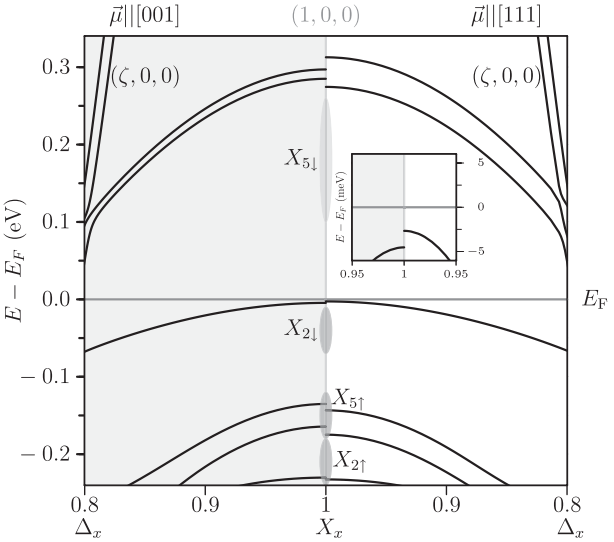

FIG. 2. Same as in Fig. 1 but around the X_x point. Note that the $X_{2\downarrow}$ band is below the Fermi energy for both magnetic-moment directions.

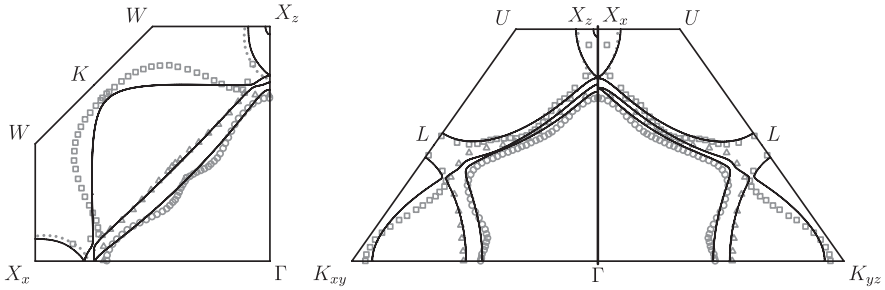

FIG. 3. Fermi-surface cuts with various planes in the Brillouin zone. Lines: Gutzwiller theory including spin-orbit coupling; squares and triangles: experimental data reported in Ref. [21]; dots: experimental data of Tsui [5].

energy [20]. For a magnetic moment along the [001] direction, however, the two states $X_{2\downarrow}$ have different energies. The $X_{2\downarrow}$ state at X_x remains below the Fermi level, whereas the corresponding state at X_z creates a new hole pocket around this X point. This is the scenario proposed by Gersdorf [8].

In Fig. 3 we show Fermi-surface cuts that we find within our Gutzwiller theory. The experimental values are taken from de Haas–van Alphen experiments by Tsui [5] and by Stark as reported in Ref. [21]. The agreement is quite satisfactory along high-symmetry lines, whereas there are significant discrepancies away from them. We do believe that the wiggles that appear in the experimental data are, in fact, spurious and we propose to redo these measurements. Now, instead of constructing the Fermi surface from those raw data, as it was done in Ref. [21], we suggest a direct comparison of the experimental de Haas–van Alphen signal with our corresponding theoretical data.

In summary, we have resolved the long-standing problem to explain theoretically the electronic and magnetic properties of elementary fcc nickel. Our calculations are based on the Gutzwiller theory which is a powerful tool for the investigation of Fermi-liquid systems with medium to strong Coulomb interaction. For such systems, state-of-the-art band-structure theories usually fail. Our results for the quasiparticle bands are in very good agreement with angle-resolved photoemission spectroscopy experiments and we find the experimental Fermi-surface topology. Furthermore, we explain the subtle effects that the spin-orbit coupling has in nickel. Our theory yields the correct magnetic anisotropy energy, and we confirm the Gersdorf scenario: The Fermi-surface topology changes around the X point (001) when the magnetic-moment direction is rotated from $\vec{\mu} \parallel [111]$ to $\vec{\mu} \parallel [001]$ by an external magnetic field.

[1] D. E. Eastman, F. J. Himpsel, and J. A. Knapp, Phys. Rev. Lett. **40**, 1514 (1978).
[2] W. Eberhardt and E. W. Plummer, Phys. Rev. B **21**, 3245 (1980).
[3] V. L. Moruzzi, J. F. Janak, and A. R. Williams, *Calculated Electronic Properties of Metals* (Pergamon, New York, 1978).
[4] J. Bünemann *et al.*, Europhys. Lett. **61**, 667 (2003).
[5] D. C. Tsui, Phys. Rev. **164**, 669 (1967).
[6] G. H. O. Daalderop, P. J. Kelly, and M. F. H. Schuurmans, Phys. Rev. B **41**, 11 919 (1990).
[7] R. Gersdorf and G. Aubert, Physica (Amsterdam) **95B+C**, 135 (1978).
[8] R. Gersdorf, Phys. Rev. Lett. **40**, 344 (1978).
[9] F. Aryasetiawan, Phys. Rev. B **46**, 13 051 (1992).
[10] A. I. Lichtenstein, M. I. Katsnelson, and G. Kotliar, Phys. Rev. Lett. **87**, 067205 (2001).
[11] S. Biermann, F. Aryasetiawan, and A. Georges, Phys. Rev. Lett. **90**, 086402 (2003).
[12] J. Bünemann, F. Gebhard, and W. Weber, in *Frontiers in Magnetic Materials*, edited by A. Narlikar (Springer, Berlin, 2005), p. 117; arXiv:cond-mat/0503332.
[13] K. M. Ho, J. Schmalian, and C. Z. Wang, Phys. Rev. B **77**, 073101 (2008); X. Deng, X. Dai, and Z. Fang, Europhys. Lett. **83**, 37 008 (2008); G.-T. Wang, X. Dai, and Z. Fang, Phys. Rev. Lett. **101**, 066403 (2008).
[14] S. Sugano, Y. Tanabe, and H. Kamimura, *Multiplets of Transition-Metal Ions in Crystals*, Pure and Applied Physics Vol. 33 (Academic, New York, 1970).
[15] M. C. Gutzwiller, Phys. Rev. Lett. **10**, 159 (1963); Phys. Rev. **134**, A923 (1964); **137**, A1726 (1965).
[16] J. Bünemann, W. Weber, and F. Gebhard, Phys. Rev. B **57**, 6896 (1998); For a comparison to slave-boson mean-field theory, see F. Lechermann *et al.*, Phys. Rev. B **76**, 155102 (2007); J. Bünemann and F. Gebhard, Phys. Rev. B **76**, 193104 (2007).
[17] J. Bünemann, F. Gebhard, and R. Thul, Phys. Rev. B **67**, 075103 (2003).
[18] In the presence of spin-orbit coupling there may also be a finite parameter $\eta_{\sigma,\sigma'}$ for a coupling between the s orbital and a certain d state. However, we found that this term does not affect the results for nickel significantly.
[19] In cubic environment there should be two different parameters ζ in (2), ζ_t and ζ_e for the couplings amongst t_{2g} and e_g orbitals, respectively. Experimentally, however, no indication for such a correction has been found; J. Callaway and C. S. Wang, Phys. Rev. B **7**, 1096 (1973).
[20] Note that in the presence of spin-orbit coupling the spin label in $X_{2\downarrow}$ is not well defined but merely refers to the main spin component of this state.
[21] C. S. Wang and J. Callaway, Phys. Rev. B **15**, 298 (1977); J. Callaway, in *Physics of Transition Metals 1980*, edited by P. Rhodes, Conference Series Notes Vol. 55 (Institute of Physics, Bristol, 1981), p. 1.